Diagnosis of Bearing Faults in Induction Machines by Vibration or Current Signals: A Critical Comparison

Fabio Immovilli, *Student Member, IEEE*, Alberto Bellini, *Member, IEEE*, Riccardo Rubini, and Carla Tassoni, *Senior Member, IEEE*

***Abstract*—Mechanical imbalances and bearing faults account for a large majority of the faults in a machine, particularly for small–medium size machines. Therefore, their diagnosis is an intensively investigated field of research. Recently, many research activities were focused on the diagnosis of bearing faults by current signals. This paper compares the bearing fault detection capability obtained with the vibration and current signals. The paper contribution is the use of a simple and effective signal processing technique for both current and vibration signals, and a theoretical analysis of the physical link between faults, modeled as a torque disturbance, and current components. The focus of the paper is on the theoretical development of the correlation between torque disturbances and the amplitude of the current components, together with a review of fault models used in the literature. Another contribution is the re-creation of realistic incipient faults and their experimental validation. Radial effects are visible only in case of large failures that result in air-gap variations. Experiments are reported that confirm the proposed approach.**

***Index Terms*—Bearings (mechanical), fault diagnosis, induction machines, signal processing.**

I. Introduction

EARLY diagnosis of faults in induction machines is an extensively investigated field for cost and maintenance savings. In fact, induction motors are still the most important rotating electric machines in industry mainly because of 1) their low price; 2) ruggedness; 3) efficiency; and 4) reliability. Many papers can be found in the literature concerning the general condition monitoring of induction machines [1]–[3] where the different fault types are analyzed. This paper focuses on bearing fault detection, which is a very attractive topic, as bearing faults are the most common failure in induction machines. The distribution of failures within the machine subassemblies is reported in many reliability survey papers [4]–[7]. A rough classification identifies four classes: 1) bearings faults; 2) stator-related faults; 3) rotor-related faults; and 4) other faults (cooling, connection, terminal boxes). Depending on the type and size of the machine, bearing faults distribution vary from about 40% to about 90% from large to small machines.

Vibration signals are usually employed to detect the presence of mechanical bearing faults. In most situations, diagnostic methods, based on the analysis of the mechanical signals, have proved their effectiveness [8]–[10]. However, in many cases, mechanical signals cannot be acquired, e.g., in harsh environment. In such conditions, electric signal measurements would be preferable.

The use of current and/or voltage signals ideally constitutes a non-invasive method to acquire information necessary to the diagnosis system and thus to ensure an effective monitoring. However, the physical link between rolling elements faults and current signatures is not clearly identified and the current components related to the faults are buried in noise, and thus, very difficult to extract without a dedicated signal processing.

This paper compares the use of the vibration and current signals for bearing faults detection, in order to check advantages and drawbacks of the two approaches in the different situations. To this aim, a testbed is realized that allows to test vibration and current signals on a machine with healthy or faulty bearings. Signal processing techniques for both cases are reviewed and compared in order to show which procedure is best suited to the different type of bearing faults. Realistic bearing faults are considered and analyzed: 1) localized simulated brinneling and 2) chemically etched single defect of the external ring of the bearing.

The paper is organized as follows. Section II reviews the mechanical behavior of the radial bearings, Section III reviews the use of the vibration signal for the detection of bearing faults, Section IV reviews the use of the current signal for the detection of bearing faults, and proposes a link between the vibration and current components, Section V reviews signals processing methods for both vibration and current signals, Section VI reports experimental results for both said signals applied to several realistic faults. Finally, conclusions are summarized in Section VII.

II. Radial Bearings Mechanical Behavior

Radial bearings consist of two concentric rings, outer and inner separated by balls or rollers, Fig. 1. Rolling elements are

Manuscript received November 28, 2008; revised July 31, 2009; accepted October 9, 2009. Date of publication May 10, 2010; date of current version July 21, 2010. Paper 2008-EMC-196.R1, presented at the 2008 Industry Applications Society Annual Meeting, Edmonton, AB, Canada, October 5–9, and approved for publication in the IEEE TRANSACTIONS ON INDUSTRY APPLICATIONS by the Electric Machines Committee of the IEEE Industry Applications Society.

F. Immovilli, A. Bellini, and R. Rubini are with the Department of Sciences and Methods of Engineering, University of Modena and Reggio Emilia, 42100 Reggio Emilia, Italy (e-mail: fabio.immovilli@unimore.it; alberto.bellini@unimore.it; riccardo.rubini@unimore.it).

C. Tassoni is with the Department of Information Engineering, University of Parma, 43100 Parma, Italy (e-mail: carla.tassoni@unipr.it).

Digital Object Identifier 10.1109/TIA.2010.2049623

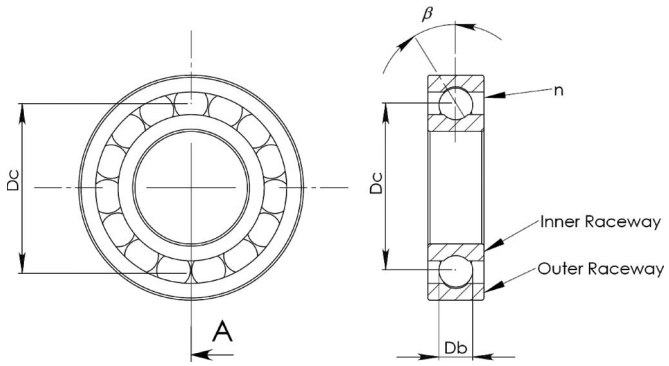

Fig. 1. Bearing structure and parameters.

bound by a cage, a structure that maintains a constant angular pitch between the adjacent rolling elements and prevents any contact. Bearing defects under normal operational conditions often occur because of material fatigue. At first, cracks appear under the surface of the tracks or of the rolling elements. Then, pitting and tearing off of material can quickly accelerate the wear of a bearing and intense vibrations are generated as a result of the repetitive impacts of the moving components on the defect.

The geometry of the radial rolling bearings and the elasticity of its components are the causes of vibrations also in healthy condition. In radial bearings, the radial stiffness depends on the angular position of the rolling elements, generating a periodical force variation due to the variation of the load distribution on the supporting balls/rollers. Hence, in the radial vibration signal spectrum, even in the healthy case, the characteristic frequency of the outer ring faults can appear. In case of pitting defects on the surface of a bearing component, the resulting local reduction of stiffness induces an instantaneous mechanical load redistribution that superimposes periodical impulses to the vibrations in the radial direction. In case of surface chemical corrosion, the change of the friction parameter in the fault zone can produce slight torsional vibrations; an analogous effect, although transitory, could be noticed in case of the early pitting fault, before the original edges of the crack are smoothed and rounded by the periodical contacts on operating conditions [8].

Vibration is a complex harmonic motion, characterized by certain values of acceleration, velocity, and displacement. Any of them can be used to obtain vibration information depending on the frequency of the signals being analyzed. Accelerometers are the most common vibration sensors for medium–high-frequency analysis. Velocimeters and displacement meters are used in particular applications where accelerometers poor low-frequency capabilities are limiting the analysis being carried out.

Here, a monoaxial accelerometer, mounted in the vertical direction, is used to pick up radial vibrations. Radial vibrations cause an air-gap permeance variation that is a complex sum of infinite number of rotating eccentricities [11]. Each machine winding works as a sensor of air-gap displacement, therefore the amplitude of the components in the vibration spectrum is expected to decrease with the square of the rotation frequency. Since the machine shaft is usually very stiff unless major fractures, the amplitude of the radial vibration and thus, permeance variation are very small. Hence, here the analysis is restricted to the effects of the bearing faults on the torsional load changes that proved to be very useful to investigate incipient faults.

III. Vibration Signals for Bearing Fault Detection

When a surface defect appears on a bearing element, impact or impulsive forces which reveal themselves in the vibration signal of the support in operating conditions, are periodic in case of the constant speed of the shaft. Hence, a periodic interaction between the rings and rolling elements occurs. If the bearing load is radial, a frequency analysis of the radial vibration signal highlights an amplitude modulation, where the carrier is any mechanical resonance, and the modulating signal is the mechanical characteristic frequency of the above described interaction phenomena

$$F_v = |f_{\mathrm{mod}} \pm k\, f_{\mathrm{car}}| \tag{1}$$

where k is an integer, f_{mod} is one of the mechanical resonance frequencies, and f_{car} is one of the mechanical characteristic frequencies, (2)–(5). A suitable demodulation of the vibration signal leads to the knowledge of the amplitude of the modulating signals.

Faults in the inner raceway, outer raceway, or rolling elements will produce unique frequency components in the machine vibration and other measured signals. These bearing fault frequencies are a function of the bearing geometry and of the operating speed [12]. If the outer ring is stationary,

$$F_C = \frac{1}{2} F_R \left(1 - \frac{D_b \cos\beta}{D_c}\right) \tag{2}$$

$$F_O = \frac{N_B}{2} F_R \left(1 - \frac{D_b \cos\beta}{D_c}\right) \tag{3}$$

$$F_I = \frac{N_B}{2} F_R \left(1 + \frac{D_b \cos\beta}{D_c}\right) \tag{4}$$

$$F_B = \frac{D_c}{D_b} F_R \left[1 - \left(\frac{D_b \cos\beta}{D_c}\right)^2\right] \tag{5}$$

where F_R is the rotor mechanical frequency, F_C is the cage fault frequency, F_I is the inner raceway fault frequency, F_O is the outer raceway fault frequency, F_B is the ball fault frequency, D_b stands for the ball diameter, D_c for the pitch diameter, N_B for the number of rolling elements, and β for the ball contact angle, Fig. 1.

Some of the mechanical problems detected by vibration spectra are the following: 1) imbalance; 2) misalignment; 3) looseness; 4) bent shaft; and 5) bearing faults.

Phase relationship between vibration at the different locations on the machine are usually employed to detect mechanical faults on the machine. As an example, the phase between the drive end bearing of the motor and the drive end bearing of the driven equipment is a very common measurement, in particular to verify misalignments. In [13], the phase between the accelerations at three different locations, i.e., drive end bearing, opposite drive end bearing, and axial reading were proposed for fault diagnosis.

TABLE I
BEARING RELATED COMPONENTS IN THE STATOR CURRENT SPECTRUM

	Model based on eccentricity [22]	Model based on torque variations [22] and on rotating eccentricities [14]
outer raceway defect	$f \pm k\,F_O$	$f \pm k\,F_O$
inner raceway defect	$f \pm F_R \pm k\,F_I$	$f \pm k\,F_I$
ball defect	$f \pm F_C \pm k\,F_B$	$f \pm k\,F_B$

IV. CURRENT SIGNALS FOR BEARING FAULT DETECTION

There are a number of papers dealing with the detection and diagnosis of faults in rolling element bearings based on the analysis of the current of the induction motor driving the machine [12]–[22]. The physical mechanism that links vibrations to motor current spectral components is however still unclear.

Finite element (FE) or winding function approaches can be used to compute machine currents and speed and torque relying on lumped mechanical parameters, typically machine-load inertia and friction, [23]–[27]. Then, the vibration spectrum can be estimated from the torque, since they share the same harmonic contents; however, the correlation between the amplitudes is not straightforward [11], [28].

Radial vibration detection via piezoelectric accelerometers measures directly the acceleration and, in case of imbalance, it is bound to the square of the mechanical rotating frequency of the machine under test, thus it is more sensitive to high-frequency phenomena. Vibration effects on machine currents are related to the air-gap variations, hence, current effects are related to displacement [14]. Because of the electromechanical filtering effects, due to the rotor inertia and winding inductance, the current is more sensitive to low-frequency phenomena.

The link between vibration and current components is presented in the literature according to two approaches.

In the first approach, the vibration component at one of the fault characteristic frequencies of the defect $f_{\rm car}$ acts on the electric machine as a torque ripple that produces a speed ripple [21], [29]. Hence, the vibration is seen as a torque component that generates in the current a chain of components at frequencies $F_{\rm be}$

$$F_{\rm be} = |f \pm k\,f_{\rm car}| \tag{6}$$

where f is the supply frequency.

According to the second approach, the effect of the vibration component on the current is modeled as a static eccentricity that is represented as the sum of a forward and backward rotating eccentricity [14].

In any case, bearing faults generate stator currents at predictable frequencies $F_{\rm be}$ (6) related to the mechanical characteristic frequencies and electrical supply frequency. The correlation between the vibration level and the magnitude of the sideband currents is tested experimentally, varying the vibration level and frequency [11]. However, the modulating components feature a very small amplitude that is buried in noise. The use of dedicated signal processing techniques is mandatory to extract efficiently the fault signature from the current signal.

In [22], a unifying approach is presented in order to define a model of stator current induced by the defect in rolling bearings elements. Here, the two aforementioned physical effects are considered separately. The effect of the radial rotor displacement is modeled as an air-gap variation, i.e., as an air-gap permeance variation, that results in a variation of the flux density in the air-gap and consequently, of the stator current. This cause-effect chain is analytically detailed for three main faults: 1) outer raceway defect; 2) inner raceway defect; and 3) ball defect. The corresponding bearing-related components in the stator current are reported in Table I and compared with [14].

However, the model based on static eccentricity only does not account for number of poles. The flux components related to eccentricity feature a pole number equal to $P \pm 1$. These waves cannot induce EMFs or currents in stator windings with P pole pairs, unless the combined effect of the static and dynamic eccentricity is considered [30]. Hence, the fault signatures at the frequencies reported in the second column of Table I are typically not visible.

In [29], the effect of torque imbalances on machine quantities are modeled; this approach is here used to investigate the relationship between torque ripple created by bearing defects and the corresponding current ripples. The fault effect is modeled as a mechanical imbalance with amplitude $\Gamma_{\rm load}$, oscillating at one of the mechanical characteristic frequencies (2)–(5) and superimposed to the constant load torque T_L. Hence, the instantaneous torque applied to the motor can be expressed as in

$$T_{\rm load}(t) = T_L + \Delta T_{\rm load}(t) = T_L + \Gamma_{\rm load}\cos(\omega_{\rm car} t). \tag{7}$$

The constant part of the electromagnetic torque $T_{\rm em}$ is equal to the load torque if mechanical losses are neglected. The effect of the torque ripple can be analyzed, neglecting electrical transient and accounting only for mechanical dynamics. If the amplitude of the torque ripple is small with respect to the main torque component, small-signals approach can be used to obtain a closed analytical model.

In [22], the electromagnetic torque is assumed constant and, as a consequence, the mechanical torque ripple appears straightforward in mechanical speed and mechanical angle. However, the modulation of the mechanical angle affects the current through induced emf, therefore, the electromagnetic torque is affected as well.

A more accurate modeling can be obtained including the electromagnetic torque ripple [29]. Let us assume that

$$T_{\rm em}(t) = T_{\rm em} + \Delta T_{\rm em}(t) = T_{\rm em} + \Gamma_{\rm em}\cos(\omega_{\rm car} t - \varphi_{\rm em}). \tag{8}$$

Specifically, the relationship between the electromagnetic torque $T_{\rm em}(t)$, the total load torque $T_{\rm load}(t)$, the mechanical speed variation and the machine-load combined inertia J is

$$J\frac{d\omega_r(t)}{dt} = T_{\rm em}(t) - T_{\rm load}(t) = T_{\rm em} - T_L + \Delta T_{\rm em}(t) - \Delta T_{\rm load}(t). \tag{9}$$

Small-signal analysis will be applied in the following, meaning that the signal can be represented by the variation around a constant bias, e.g., $\omega_r(t) = \omega_r + \Delta\omega_r(t)$. With small-signal analysis, (9) becomes

$$J\frac{d\Delta\omega_r(t)}{dt} = \Delta T_{\rm em}(t) - \Gamma_{\rm load}\cos(\omega_{\rm car}t). \tag{10}$$

Let us assume a linear shape for the electromagnetic torque in steady-state conditions

$$\Delta T_{\rm em}(t) = -K_T\Delta\omega_r(t) \tag{11}$$

where the gain K_T between the torque and speed variations can be approximately computed from the usual steady-state equivalent circuit of the machine, neglecting the following: 1) the no-load current; 2) the stator resistance; and 3) the leakage reactance. Under these assumptions, the proposed model is valid only in normal operating conditions, e.g., near rated load. From (12), we can estimate K_T as in

$$T_{\rm em} \simeq \frac{3P}{\omega_s}\frac{V^2}{R_r}\left(1 - P\frac{\omega_r}{\omega_s}\right) \tag{12}$$

$$K_T = \frac{3P^2}{\omega_s^2}\frac{V^2}{R_r} \tag{13}$$

where R_r is the rotor resistance. Obviously, a more accurate value of K_T can be estimated from the actual shape between $T_{\rm em}$ and ω_r in correspondence to the operating condition.

Replacing K_T into (11) and (10), a first-order differential equation is obtained that links the speed ripple $\Delta\omega_r$ and the oscillating load torque

$$J\frac{d\Delta\omega_r(t)}{dt} + K_T\Delta\omega_r(t) = -\Gamma_{\rm load}\cos(\omega_{\rm car}t). \tag{14}$$

The speed ripple is obtained solving

$$\Delta\omega_r(t) = -\frac{\Gamma_{\rm load}}{\sqrt{K_T^2 + \omega_{\rm car}^2J^2}}\cos(\omega_{\rm car}t - \varphi_{\rm em}) \tag{15}$$

where

$$\varphi_{\rm em} = \arctan\frac{\omega_{\rm car}J}{K_T}.$$

Replacing (15) into (11),

$$\Delta T_{\rm em}(t) = -\frac{K_T\Gamma_{\rm load}}{\sqrt{K_T^2 + \omega_{\rm car}^2J^2}}\cos(\omega_{\rm car}t - \varphi_{\rm em}). \tag{16}$$

Therefore, the electromechanical torque ripple amplitude and its angle are

$$\Gamma_{\rm em} = \frac{K_T\Gamma_{\rm load}}{\sqrt{K_T^2 + \omega_{\rm car}^2J^2}}, \quad \varphi_{\rm em} = \arctan\frac{\omega_{\rm car}J}{K_T}.$$

Neglecting mechanical losses, it becomes

$$\frac{\Gamma_{\rm em}}{T_{\rm em}} = \frac{K_T}{\sqrt{K_T^2 + \omega_{\rm car}^2J^2}}\frac{\Gamma_{\rm load}}{T_L}. \tag{17}$$

The ripple of the electromagnetic torque at $\omega_{\rm car}$ produces a current modulation ΔI and a flux modulation $\Delta\Phi$ at the same pulsation. Specifically, a relationship can be found between the torque ripple normalized to the torque fundamental component and the normalized current and flux ripples. The space vector of the stator current is defined as $\vec{i}_s = I_d + \jmath I_q$, where the d-axis is in phase with the voltage, while the q-axis is in quadrature. Similarly, $\vec{\Phi}_s = \Phi_d + \jmath\Phi_q$. The scalar value of the torque is computed relying on space vectors

$$T_{\rm em} = p\,{\rm Im}\left[\vec{\Phi}_s\vec{i}_s^{\star}\right] = 3p\Phi_qI_d. \tag{18}$$

Then, replacing (18) into (17),

$$\frac{\Delta T_{\rm em}}{T_{\rm em}} = \frac{3p\left(\Phi_q + \Delta\Phi_q\right)\left(I_d + \Delta I_d\right)\right)}{3p\Phi_qI_d} \simeq \frac{\Delta\Phi_q}{\Phi_q} + \frac{\Delta I_d}{I_d}. \tag{19}$$

Assuming that $I_d = I\cos\phi$, where $\cos\phi$ is the power factor and that $\Delta I_d = \Delta I$, the torque ripple can be expressed as

$$\frac{\Gamma_{\rm em}}{T_{\rm em}} \simeq \frac{\Delta I}{I\cos\phi} + \frac{\Delta\Phi}{\Phi}. \tag{20}$$

Simulation and experiments confirm that the flux ripple can be neglected in (20) [31], thus, the torque ripple becomes

$$\frac{\Gamma_{\rm em}}{T_{\rm em}} \simeq \frac{\Delta I}{I\cos\phi} \tag{21}$$

where I is the amplitude of the current fundamental component. In the stator current, two components at $f \pm f_{\rm car}$ appear. Hence, from (17)

$$\frac{\Delta I}{I\cos\phi} = \frac{K_T}{\sqrt{K_T^2 + \omega_{\rm car}^2J^2}}\frac{\Gamma_{\rm load}}{T_L}. \tag{22}$$

From (22), it turns out that the components in the stator current related to the bearing defects appear at frequencies consistent with (6). However, the amplitude of the torque oscillation $\Gamma_{\rm load}$ is very small for real defects, and the amplitude of the signatures in the current is a fraction of $\Gamma_{\rm load}$. The following considerations hold for small–medium machines, where K_T ranges from one to ten, while $J\omega_{\rm car}$ is difficult to estimate. It depends on many factors, including mechanical inertia and mechanical characteristic frequency of defects; however, it is possible to assume that $J\omega_{\rm car}$ is much larger that K_T at least for the mechanical characteristic frequencies (2)–(4). Therefore, the coefficient between the torque ripple and the current modulation is a damping coefficient.

In summary, it is very difficult to retrieve bearing fault signatures in the current, while it is possible to retrieve the ripple components in the torque signal using a torque meter with sufficient sensitivity. In [32], vibration and torque analysis are reviewed in order to monitor the conditions of rolling elements bearings with on-field data. Both techniques were successfully employed to detect incipient faults. The attenuation between the torque ripple and the current modulation is enhanced increasing the frequency, hence, in the current, only defects characterized by a relatively low-mechanical-frequency rate can be detected. This is consistent with the analysis made in [14].

V. Signal Processing Methods for the Detection of Rolling Elements Faults

For both vibration and current signals, a proper signal processing is required to retrieve the modulating signals, i.e., the mechanical characteristic frequencies. Here, the use of the traditional discrete Fourier transform (DFT), Hilbert transformation, and envelope analysis are critically compared. With traditional DFT, the spectrum of the machine input current is computed and the components (6), (1) are monitored to check the variation with respect to the healthy case. The other techniques are briefly reviewed in the following.

A. Hilbert Transformation

The procedure to identify the components in the vibration signal spectrum related to the bearing faults relying on Hilbert transformation is as follows [10]. 1) Compute the Fourier Transformation of the vibration time signal. 2) The vibration signal is bandpass-filtered in order to obtain a reduced spectrum around $f_{\rm mod}$. 3) Compute the Hilbert transformation of the bandpass-filtered signal. 4) Compute the Fourier Transformation of the analytic signal obtained through Hilbert transformation. Hence, it is possible to retrieve the components at k $f_{\rm car}$. The variations of their amplitudes, with respect to the healthy case, state the occurrence of the related bearing fault.

Item 1) allows to isolate the resonance frequency of the system in our specific setup. However, in on-field measurements, it is impossible to distinguish resonant frequencies and forced frequencies of unknown source. Hence, the Fourier Transformation of a signal under steady-state conditions is not a reliable tool. In a complex system, two methods can be used in order to assess the resonant frequencies: 1) the coast-down test; and 2) the bump test.

The former is realized setting up "streaming" the spectrum obtained with the vibration tester and then turning off the motor. Any resonant frequency between steady-state running frequency and zero will be excited by the inherent mechanical unbalance, showing an enhanced peak when the speed peak sweeps through this particular mechanical resonance. The drawback of this technique is that resonant frequencies will be excited by the inherent first and perhaps second-speed harmonics. Hence, higher resonant frequencies cannot be found.

The bump test is realized keeping the machine at standstill and hitting it with a mallet; the consequent oscillation will portray the various resonant components.

B. Envelope Analysis

Another approach to separate modulation signals from the carrier is here presented. This method can be used to obtain the modulating signals related to mechanical fault characteristic frequencies with higher accuracy, increasing the signal-to-noise ratio of the results [33]. With respect to the use of the Hilbert transformation, this method features a few advantages: 1) bandpass filtering is not required; 2) the method is effective even without the knowledge of the carrier; and 3) the computational cost is lower.

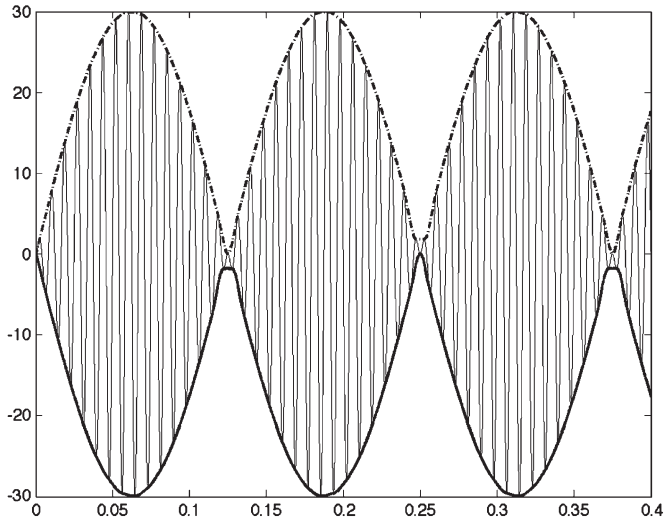

Fig. 2. Example of envelope analysis. upp_e dashed line, low_e solid line.

The procedure is detailed in the following. The signal is processed in order to compute the upper and lower envelope, upp_e, low_e, respectively, Fig. 2. In case of the amplitude modulation with modulation index lower than one, the modulating signal is computed by $m_s(t) = \text{upp}_e - \text{low}_e$ and the carrier by $c_s(t) = \text{upp}_e + \text{low}_e$. This reduces common mode errors. Then, the spectrum of $m_s(t)$ is computed that provides the amplitudes of the components at the mechanical frequencies of the faults. Their variations with respect to the healthy case, state the occurrence of the related bearing fault.

In summary, the envelope analysis identifies all the local maxima of the acquired signal and then uses linear interpolation to obtain the upper envelope of the signal. The same procedure, employing local minima, applies to the lower envelope. The modulating signal is obtained by the difference of the two separate envelopes. The sum of the two envelopes (upper and lower) represents the asymmetry of the modulation, caused by the offset and common mode noise in the acquired signal.

VI. Experimental Results

A small induction machine is used to validate the proposed approach. Three identical rotors are prepared: one rotor carries healthy bearings, while the others mount one artificially damaged bearing each. The nameplate of the machine is 1.5-kW three-phase induction machine, with $V_{\rm rms} = 380$ V, $N_b = 28$ rotor bars, and $P = 2$ pole pairs. Rated slip and frequency are $s = 7\%$ and $f = 50$ Hz, $(sf = 3.5$ Hz). The rotor is carried by two bearings, one of which is defective.

The reported bearing parameters are taken from the datasheet while the ball contact angle β is estimated from various measurements. The mounted bearing is a KBC 6205, with an outside diameter of 52 mm, an inside diameter of 25 mm, and nine balls, $D_c = 40.02$ mm, $D_b = 8.04$ mm, $\cos\beta = 0.99$, and $\beta = 0.14$ rad. Hence, the mechanical fault characteristic frequencies (2)–(5) are reported in Table II for $f = 30$ and 50 Hz.

Two types of damages were artificially made on the bearings:

- a simulated brinelling defect, generated applying a mechanical load of 4 T (40 kN) to the bearing, Fig. 3-left:

TABLE II
MECHANICAL CHARACTERISTIC FREQUENCIES (IN HERTZ) FOR BEARING DEFECTS

f	F_O	F_I	F_B	F_C
30	54.1	80.9	71.7	6
50	90.1	134.9	119.5	10

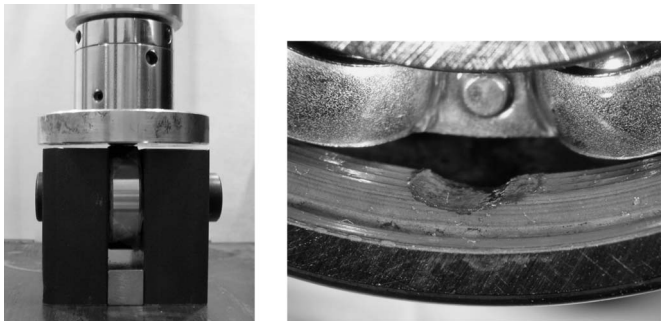

Fig. 3. (Left) Photograph of the test setup for making bearing brinelling damages. (Right) Microscope photograph of the single defect created by chemical etching.

it is expected that the mechanical frequencies F_B and F_O are generated;

- a single defect on the outer raceway, created by chemical etching of the bearing outer race, Fig. 3-right. The bearing was degreased, waxed by immersion in molten paraffin, then the protecting paraffin on a small portion of the outer race was removed to expose the bare metal. The prepared bearing was immersed overnight in ferric chloride for the etching process to take place. The protective paraffin was then molten away, and the bearing was cleaned and relubricated. The resulting defect is like a shallow groove or fluting with rough surfaces, running perpendicular across the outer race. Therefore, in this case, it is expected that the characteristic frequency at F_O appears because of the outer raceway fault.

The above defects were created in order to simulate real cases, trying to reproduce a single defect. Measurements were taken early after the creation of the defect, assuming that over time it might degenerate into a generalized roughness, preventing the detection of distinctive signatures.

The machine was operated at a constant volts-per-hertz ratio at loads between zero and rated load. A power inverter, operated at a switching frequency of 13 kHz, generates the supply voltages. The testbed allows for controlling the torque applied to the machine under test, Fig. 4. Machine currents, voltages, speed, torque, and vibration signals are sampled at $F_s = 20$ kHz. A monoaxial accelerometer is used to pick up radial vibration: ICP piezoelectric accelerometer model 352C41 with a sensitivity equal to 10 $\mathrm{mV/ms^2}$ and a frequency range from 0.3 to 15 000 Hz.

A. Healthy Machine

Current and vibration signals were sampled with the above described testbed and they were processed with DFT, Hilbert transformation, and with the envelope analysis with the healthy rotor.

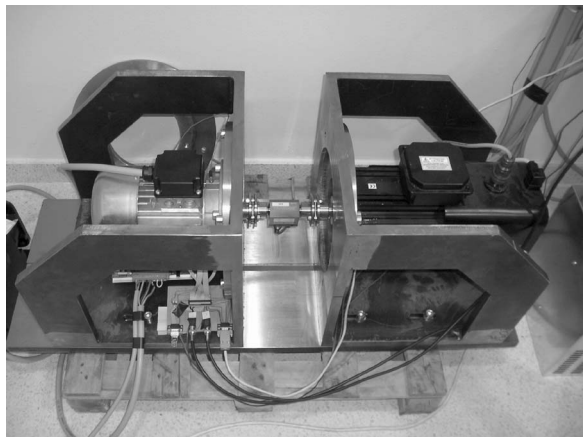

Fig. 4. Photograph of the testbed used for the bearing fault detection.

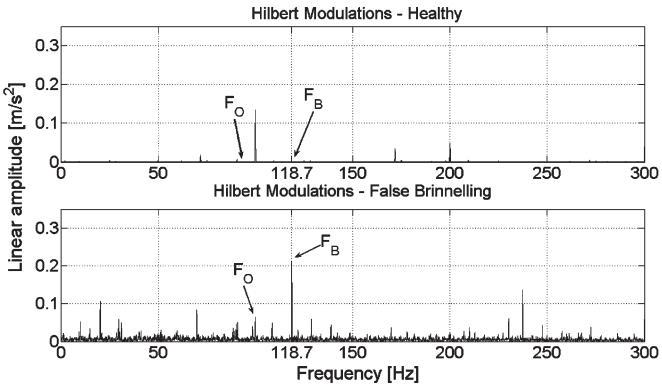

Fig. 5. (Top) Spectrum of the vibration signal of the machine after Hilbert transformation. Supply frequency is 50 Hz. Healthy machine. (Bottom) Machine with simulated brinelling.

The vibration signal is related to the rotational speed of the shaft and to the radial load on the bearing surfaces. No significant difference exists between the experiments at no-load and at rated load, confirming the independence of the vibration signal from the torque transmitted by the shaft. Since the amplitudes of the vibration fault signature are independent of the torque load of the machine, in the following, the analysis of the experimental data is restricted to no-load condition.

B. Brinelling

The same testbed was used to sample electric and mechanical signal with the bearing affected by simulated brinelling. The processing techniques presented in Section V were used to extract significant information from the signals spectrum.

The spectrum of the vibration signal obtained after Hilbert transformation is reported in Fig. 5, where healthy and faulty cases are compared. It turns out that a component F_B (ball fault frequency) appears clearly in the spectrum of the machine in the case of simulated brinelling, and that a component at F_O (outer raceway fault frequency) is slightly increased. The spectrum of the modulating signal $m_s(t)$ obtained after envelope analysis of the vibration signal is reported in Fig. 6 where the healthy and faulty cases are compared. It can be noticed that the sensitivity of the envelope analysis is higher than that of the Hilbert transformation.

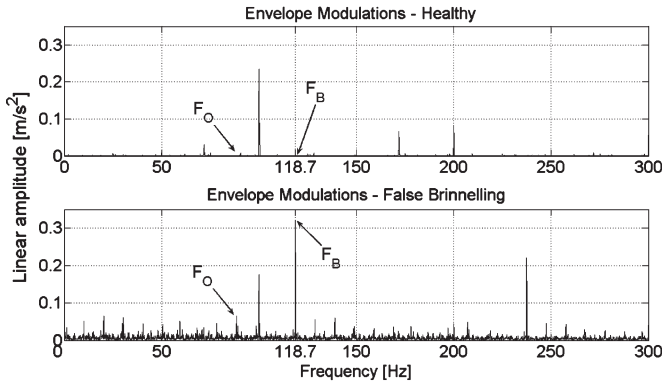

Fig. 6. (Top) Spectrum of the modulating signals of the machine after envelope analysis of the vibration signal. Supply frequency is 50 Hz. Healthy machine. (Bottom) Machine with simulated brinelling.

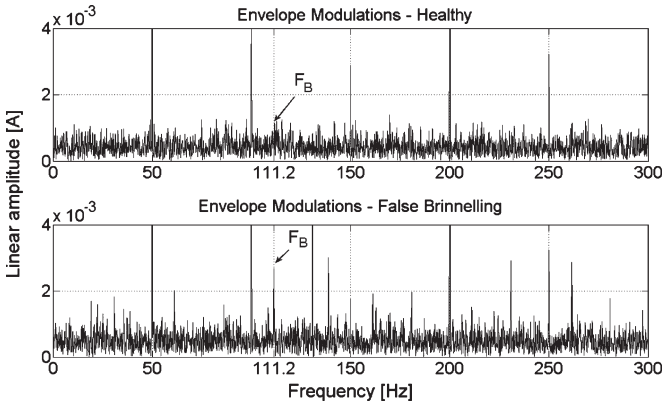

Fig. 7. (Top) Spectrum of the modulating signals of the machine current after envelope analysis of the line current signal. Supply frequency is 50 Hz. Healthy machine. (Bottom) Machine with simulated brinelling.

Current signals were measured under the same conditions. The spectrum of the modulating signal $m_s(t)$ obtained after envelope analysis of the current signal is reported in Fig. 7, where healthy and faulty cases are compared. Results obtained under the same conditions with Hilbert transformation are omitted as the envelope analysis proved to be more sensitive. A component close to the ball frequency F_B (ball fault frequency) appears.

C. Chemically Etched Single-Point Defect

The same testbed was used to sample the electric and mechanical signals in the case of a bearing with a single defect on the outer raceway, realized with chemical etching. The spectrum of the modulating signal $m_s(t)$ obtained after envelope analysis of the vibration signal is reported in Fig. 8, where healthy and faulty cases are compared. It turns out that a component at F_O (outer raceway fault frequency) appears clearly in the spectrum of the machine with bearing with a single defect. The presence of the upper harmonics is a typical feature of this type of defect.

Current signals were measured under the same conditions. The spectrum of the current signal is reported in Fig. 9, in case of a machine with a single defect. Because of the relatively high characteristic frequency of the defect, it is hard to retrieve some fault information, even with signal processing techniques. In this case, the current signal is not a reliable indicator of the outer raceway faults.

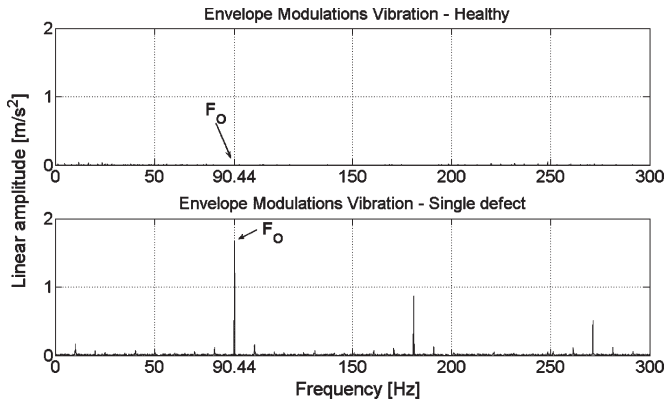

Fig. 8. (Top) Spectrum of the modulating signals of the machine after envelope analysis of the vibration signal. Supply frequency is 50 Hz. Healthy machine. (Bottom) Machine with a chemically etched single defect.

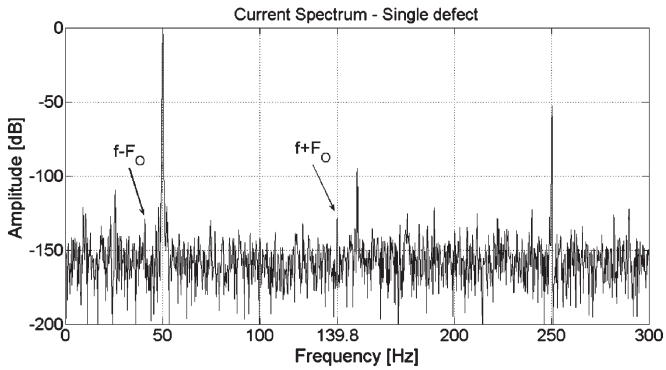

Fig. 9. Spectrum of a line current signal of the machine with a chemically etched single defect. Supply frequency is 50 Hz.

D. Space Vector Analysis of the Current

It could be expected that the occurrence of a failure in the outer raceway, that is asymmetrical with respect to the three-phase stator circuits, could be highlighted by space vector analysis. To this aim, the current signals were processed, (23), in order to assess the presence/increase of defect harmonics modulation in the spectrum of the currents space vector

$$[ht!]\vec{i}_s = K\left[i_u(t) + i_v(t)\alpha + i_w(t)\alpha^2\right] \tag{23}$$

where $\alpha = e^{\jmath(2\pi/3)}$ and $K = \sqrt{3/2}$.

Figs. 10 and 11 show the space vector spectra of the motor currents for the healthy machine and for the machine with a single-point chemically etched defect, with a supply frequency of 50 and 30 Hz, respectively. Spectra are normalized to the amplitude of the fundamental component and, as expected, the amplitude of the positive component at frequency f is remarkably larger than the corresponding component at $-f$ (-80 dB), while the amplitudes of components at $\pm 3f$ are similar as it is an alternative field; eventually, the amplitude of the negative component at $-5f$ is larger than the corresponding component at $5f$ as it is a counter-rotating field. As stated before, no useful information can be obtained from current signals, because the effects of the real failures are buried in noise.

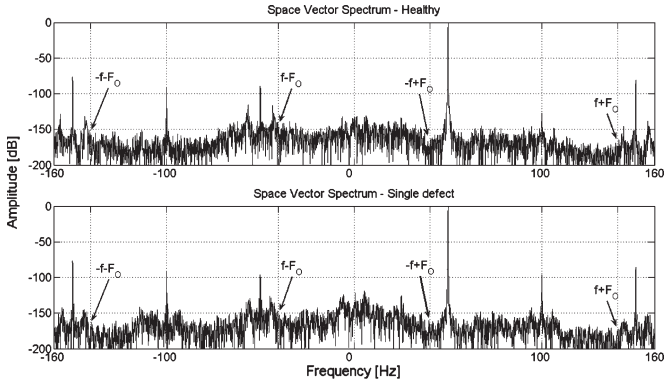

Fig. 10. (Top) Spectrum of the currents space vector of the machine current signal supplied at 50 Hz. Healthy machine. (Bottom) Machine with a chemically etched single defect.

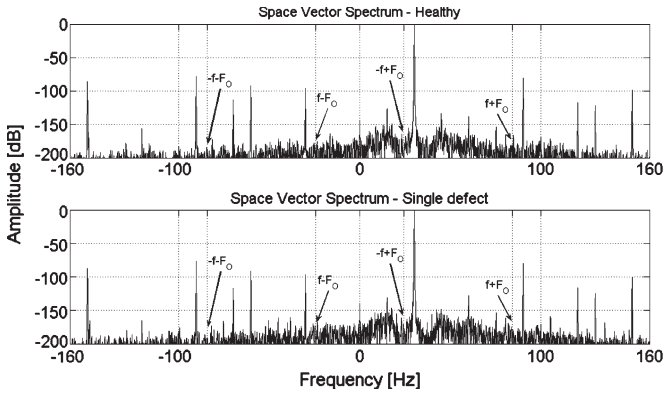

Fig. 11. (Top) Spectrum of the currents space vector of the machine supplied at 30 Hz. Healthy machine. (Bottom) Machine with a chemically etched single defect.

Another test at a supply frequency of 30 Hz shows a lower noise, but again no information of bearing fault is distinguishable.

E. Effects of Torque Ripple

Another set of experiments was conducted to validate the theoretical analysis of Section IV. In the previously detailed testbed, the brake machine was used to spin the machine under test. A torque meter was interposed between the two machines in order to measure the torque ripple created by the bearing defects. The torque meter used is a Staiger-Mohilo 4502A20R, employing strain gage technology and contactless torque signal transmission from the rotating shaft via frequency modulation. Torque meter measuring range is ± 20 Nm and its accuracy is ± 2 mNm.

The bearing with a chemically etched single-point defect was used and compared with a healthy bearing. In the torque signal, a component at F_O is clearly present, as reported in Figs. 12 and 13, showing test runs at 30 Hz and 50 Hz, respectively. The torque ripple increases with supply frequency and thus, with the speed of the machine; this is probably due to the mechanical impact between the rolling element and the defect on the outer race. At higher speed, the kinetic energy increases and it exerts higher contact pressure on the outer ring, thus the more violent impact dissipates a greater amount of kinetic energy and causes

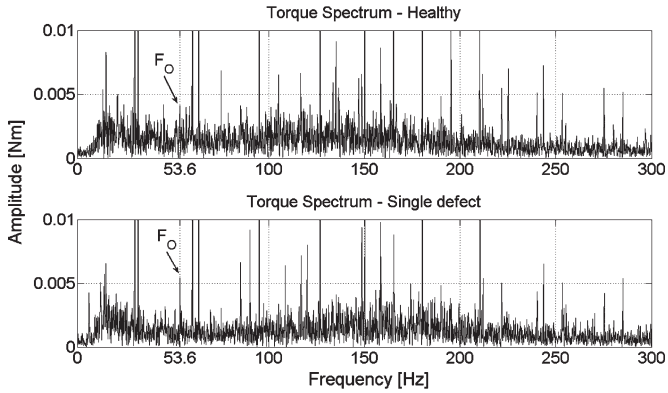

Fig. 12. (Top) Spectrum of the torque signal of the machine supplied at 30 Hz. Healthy machine. (Bottom) Machine with a chemically etched single defect.

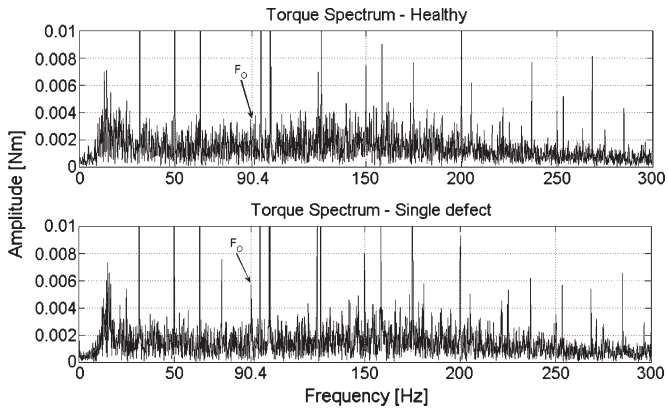

Fig. 13. (Top) Spectrum of the torque signal of the machine supplied at 50 Hz. Healthy machine. (Bottom) Machine a chemically etched with single defect.

greater torque ripple. At 30 Hz, the amplitude of the torque ripple varies from about 2 mNm to 5.5 mNm, while at 50 Hz, the amplitude of the torque ripple varies from about 1.5 mNm to 6 mNm.

Since the torque ripple due to the bearing fault is independent of the torque load on the machine, when the motor is running in standard conditions (e.g., near rated load), from (22), the current ripple referred to the active current amplitude is 0.2–0.5 mA at 50 Hz. Hence, the current component at $f_r + F_O$ is not visible, as it would require a current sensor with resolution and sensitivity that is usually not available in industrial drives. In fact, in the spectrum of a stator current signal, no signatures can be detected as reported in Fig. 14. Similarly, the modulating signals related to the defect cannot be retrieved in the result of the envelope analysis as reported by Fig. 15.

On the other hand, for bearing cage faults, the ratio between the ripple of torque and currents is about the same, hence it could be possible to detect the current component at $f + F_C$, provided that a current sensor with a suitable sensitivity (around mA) is available.

VII. Conclusion

In this paper a theoretical analysis of the relationship between torque disturbances and current components amplitudes

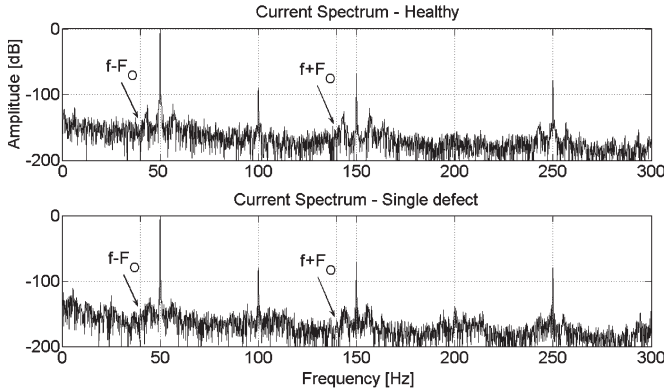

Fig. 14. (Top) Spectrum of the line current signal of the machine. Healthy machine. (Bottom) Machine with a chemically etched single defect.

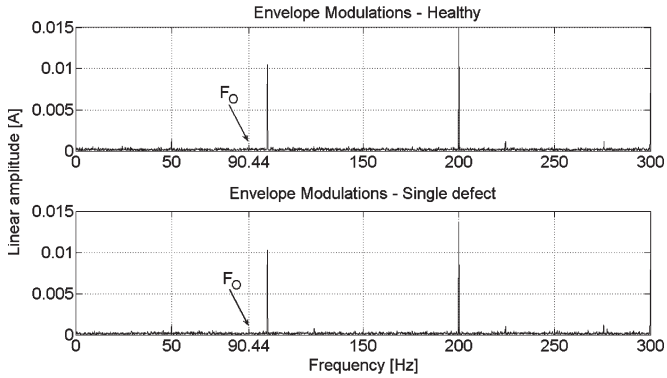

Fig. 15. (Top) Spectrum of the modulating signals of the machine current after envelope analysis of the line current signal. Healthy machine. (Bottom) Machine with a chemically etched single defect.

is developed and presented, together with a review of fault models used in the literature for the diagnosis of bearing faults in induction machines.

Modeling the fault as a torque disturbance helps to predict the frequencies of the components (signatures) in the stator current spectrum related to each rolling element defects and to make a quantitative analysis of their amplitudes. Signal processing techniques used to improve fault detection are reviewed, among them is the envelope analysis which was investigated, showing that it rivals Hilbert transformation in terms of the sensitivity at a reduced computational cost. As expected, because of the different nature of the vibration and current, the detection of the bearing faults with current signal is effective only for those faults whose characteristic frequency is quite low. Hence, it is possible to use current signal as a reliable media to detect bearing faults only in specific operating conditions. On the other hand, vibration signals are a robust indicator for bearing defects provided that a suitable processing is made.

REFERENCES

[1] A. Bellini, F. Filippetti, C. Tassoni, and G. A. Capolino, "Advances in diagnostic techniques for induction machines," *IEEE Trans. Ind. Electron.*, vol. 55, no. 12, pp. 4109–4126, Dec. 2008.

[2] S. Nandi, H. A. Toliyat, and X. Li, "Condition monitoring and fault diagnosis of electrical motors—A review," *IEEE Trans. Energy Convers.*, vol. 20, no. 4, pp. 719–729, Dec. 2005.

[3] M. El Hachemi Benbouzid, "A review of induction motors signature analysis as a medium for faults detection," *IEEE Trans. Ind. Electron.*, vol. 47, no. 5, pp. 984–993, Oct. 2000.

[4] O. V. Thorsen and M. Dalva, "A survey of faults on induction motors in offshore oil industry, petrochemical industry, gas terminals, and oil refineries," *IEEE Trans. Ind. Appl.*, vol. 31, no. 5, pp. 1186–1196, Sep./Oct. 1995.

[5] P. O'Donnell, "Report of large motor reliability survey of industrial and commercial installations, part I," *IEEE Trans. Ind. Appl.*, vol. IA-21, no. 4, pp. 853–864, Jul. 1985.

[6] P. O'Donnell, "Report of large motor reliability survey of industrial and commercial installations, part II," *IEEE Trans. Ind. Appl.*, vol. IA-21, no. 4, pp. 865–872, Jul. 1985.

[7] A. H. Bonnett, "Root cause AC motor failure analysis with a focus on shaft failures," *IEEE Trans. Ind. Appl.*, vol. 36, no. 5, pp. 1435–1448, Sep./Oct. 2000.

[8] R. Rubini and U. Meneghetti, "Application of the envelope and wavelet transform analysis for the diagnosis of incipient faults in ball bearings," *Mech. Syst. Signal Process.*, vol. 15, no. 2, pp. 287–302, Mar. 2001.

[9] J. R. Stack, T. G. Habetler, and R. G. Harley, "Fault-signature modeling and detection of inner-race bearing faults," *IEEE Trans. Ind. Appl.*, vol. 42, no. 1, pp. 61–68, Jan./Feb. 2006.

[10] J. R. Stack, T. G. Habetler, and R. G. Harley, "An amplitude modulation detector for fault diagnosis in rolling element bearing," *IEEE Trans. Ind. Electron.*, vol. 51, no. 5, pp. 1097–1102, Oct. 2004.

[11] C. M. Riley, B. K. Lin, T. G. Habetler, and G. B. Kliman, "Stator current harmonics and their causal vibrations: A preliminary investigation of sensorless vibration monitoring applications," *IEEE Trans. Ind. Appl.*, vol. 35, no. 1, pp. 94–99, Jan./Feb. 1999.

[12] R. R. Schoen, T. G. Habetler, F. Kamran, and R. G. Bartfield, "Motor bearing damage detection using stator current monitoring," *IEEE Trans. Ind. Appl.*, vol. 31, no. 6, pp. 1274–1279, Nov./Dec. 1995.

[13] *IEEE Guide for Induction Machinery Maintenance Testing and Failure Analysis*, IEEE Std. 1415-2006, pp.c1-58, Apr. 30, 2007.

[14] C. M. Riley, B. K. Lin, T. G. Habetler, and R. R. Schoen, "A method for sensorless on-line vibration monitoring of induction machines," *IEEE Trans. Ind. Appl.*, vol. 34, no. 6, pp. 1240–1245, Nov./Dec. 1998.

[15] J. R. Stack, T. G. Habetler, and R. G. Harley, "Bearing fault detection via autoregressive stator current modeling," *IEEE Trans. Ind. Appl.*, vol. 40, no. 3, pp. 740–747, May/Jun. 2004.

[16] J. R. Stack, T. G. Habetler, and R. G. Harley, "Fault classification and fault signature production for rolling element bearings in electric machines," *IEEE Trans. Ind. Appl.*, vol. 40, no. 3, pp. 735–739, May/Jun. 2004.

[17] M. Blodt, P. Granjon, B. Raison, and G. Rostaing, "Models for bearing damage detection in induction motors using stator current monitoring," in *Proc. IEEE Int. Symp. Ind. Electron.*, May 2004, vol. 1, pp. 383–388.

[18] O. Duque, M. Perez, and D. Morinigo, "Detection of bearing faults in cage induction motors fed by frequency converter using spectral analysis of line current," in *Proc. IEEE IEMDC*, May 2005, pp. 17–22.

[19] J. L. H. Silva and A. J. M. Cardoso, "Bearing failures diagnosis in three-phase induction motors by extended Park's vector approach," in *Proc. IEEE IECON*, Nov. 2005, pp. 2591–2596.

[20] L. Sun and B. Xu, "An improvement of stator current based detection of bearing fault in induction motors," in *Conf. Rec. IEEE IAS Annu. Meeting*, New Orleans, LA, Sep. 2007, pp. 2277–2281.

[21] M. Blodt, D. Bonacci, J. Regnier, M. Chabert, and J. Faucher, "On-line monitoring of mechanical faults in variable-speed induction motor drives using the Wigner distribution," *IEEE Trans. Ind. Electron.*, vol. 55, no. 2, pp. 522–533, Feb. 2008.

[22] M. Blodt, P. Granjon, B. Raison, and G. Rostaing, "Models for bearing damage detection in induction motors using stator current monitoring," *IEEE Trans. Ind. Electron.*, vol. 55, no. 4, pp. 1813–1822, Apr. 2008.

[23] H. A. Toliyat and T. A. Lipo, "Transient analysis of cage induction machines under stator, rotor bar and end ring faults," *IEEE Trans. Energy Convers.*, vol. 10, no. 2, pp. 241–247, Jun. 1995.

[24] J. F. Watson and D. G. Dorrell, "The use of finite element methods to improve techniques for the early detection of faults in 3-phase induction motors," *IEEE Trans. Energy Convers.*, vol. 14, no. 3, pp. 655–660, Sep. 1999.

[25] G. Houdouin, G. Barakat, B. Dakyo, and E. Destobbeleer, "A winding function theory based global method for the simulation of faulty induction machines," in *Proc. IEEE IEMDC*, Jun. 2003, vol. 1, pp. 297–303.

[26] A. Ghoggal, M. Sahraoui, A. Aboubou, S. E. Zouzou, and H. Razik, "An improved model of the induction machine dedicated to faults detection extension of the modified winding function," in *Proc. IEEE ICIT*, Dec. 2005, pp. 191–196.

[27] J. Faiz, B. M. Ebrahimi, B. Akin, and H. A. Toliyat, "Finite-element transient analysis of induction motors under mixed eccentricity fault," *IEEE Trans. Magn.*, vol. 44, no. 1, pp. 66–74, Jan. 2008.
[28] C. M. Riley, B. K. Lin, T. G. Habetler, and G. B. Kliman, "Stator current-based sensorless vibration monitoring of induction motors," in *Proc. IEEE APEC*, Feb. 1997, vol. 1, pp. 142–147.
[29] G. Salles, F. Filippetti, C. Tassoni, G. Crellet, and G. Franceschini, "Monitoring of induction motor load by neural network techniques," *IEEE Trans. Power Electron.*, vol. 15, no. 4, pp. 762–768, Jul. 2000.
[30] D. G. Dorrell, W. T. Thomson, and S. Roach, "Analysis of airgap flux, current, and vibration signals as a function of the combination of static and dynamic airgap eccentricity in 3-phase induction motors," *IEEE Trans. Ind. Appl.*, vol. 33, no. 1, pp. 24–34, Jan./Feb. 1997.
[31] C. Concari, G. Franceschini, C. Tassoni, and A. Bellini, "Torque and field currents peculiarities under different induction machine troubles," in *Proc. IEEE Int. SDEMPED*, Sep. 2007, pp. 302–308.
[32] H. Smith, E. Wiedenbrug, and M. Lind, "Rotating element bearing diagnostics in a nuclear power plant: Comparing vibration and torque techniques," in *Proc. IEEE Int. SDEMPED*, Sep. 2007, pp. 17–22.
[33] R. B. Randall, J. Antoni, and S. Chobsaard, "A comparison of cyclostationary and envelope analysis in the diagnostics of rolling element bearings," in *Proc. IEEE ICASSP*, Istanbul, Turkey, Jun. 2000, vol. 6, pp. 3882–3885.

Fabio Immovilli (S'08) was born in Italy on March 11, 1981. He received the Dr. Eng. degree in mechatronic engineering from the University of Modena and Reggio Emilia, Reggio Emilia, Italy, in 2006, where he is currently working toward the Ph.D. degree in mechatronic engineering in the Department of Sciences and Methods of Engineering.

In 2009, he was a Visiting Scholar at the University of Nottingham, Nottingham, U.K. His research interests include electric machine diagnostics, power converters, machines for energy conversion from renewable energy sources, and thermoacoustics. He holds one international industrial patent.

Alberto Bellini (S'96–M'99) was born in Italy in 1969. He received the Laurea (M.S.) degree in electronic engineering and the Ph.D. degree in computer science and electronic engineering from the University of Bologna, Bologna, Italy, in 1994 and 1998, respectively.

From 1999 to 2004, he was with the University of Parma, Parma, Italy. He was an Honorary Scholar at the University of Wisconsin, Madison, during 2000. Since 2004, he has been at the University of Modena and Reggio Emilia, Reggio Emilia, Italy, where he is currently an Assistant Professor of electric machines and drives in the Department of Sciences and Methods of Engineering. His research interests include power electronics, signal processing for audio and industrial applications, and electric drive design and diagnosis. He is the author or coauthor of more than 80 papers and one textbook, and is the holder of three industrial patents.

Dr. Bellini was the recipient of the First Prize Paper Award from the Electric Machines Committee of the IEEE Industry Applications Society in 2001. He is a member of the Italian Association of Converters, Electrical Machines and Drives (CMAE). He is an Associate Editor for the IEEE TRANSACTIONS ON INDUSTRIAL ELECTRONICS.

Riccardo Rubini received the M.S. degree in mechanical engineering and the Ph.D. degree in mechanics of machines from the University of Bologna, Bologna, Italy, in 1993 and 1997, respectively.

In 1996, he was a Visiting Researcher at the University of Technology of Compiègne, Compiègne, France. From 2000 to 2004, he was an Assistant Professor in the Faculty of Engineering, University of Bologna. He is currently an Associate Professor in the Department of Sciences and Methods of Engineering, University of Reggio Emilia, Reggio Emilia, Italy. His research interests are focused on the fields of dynamics of machines and advanced techniques for the monitoring and diagnostics of mechanical components.

Carla Tassoni (SM'97) was born in in Bologna, Italy, in 1942. She received the Master's degree in electrical engineering from the University of Bologna, Bologna, in 1966.

She was with the University of Bologna, first as an Assistant Professor and then as an Associate Professor of electrical machines in the Department of Electric Engineering. She is currently a Full Professor of electrical engineering at the University of Parma, Parma, Italy. She is the author or coauthor of more than 150 scientific papers. Her main research interests include simulation and modeling of electric systems and applications of diagnostic techniques.